The Meteoritical Society

Meteoritics & Planetary Science 1–21 (2020)
doi: 10.1111/maps.13486

Classification of CM chondrite breccias—Implications for the evaluation of samples from the OSIRIS-REx and Hayabusa 2 missions

Sarah LENTFORT[1], Addi BISCHOFF[1]*, Samuel EBERT[1,2], and Markus PATZEK[1]

[1]Institut für Planetologie, Westfälische Wilhelms-Universität Münster, Wilhelm-Klemm Str. 10, D-48149 Münster, Germany
[2]SOEST/HIGP, University of Hawaii at Manoa, University of Hawai'i, 1680 East-West Road, POST 516B, Honolulu, HI 96822, USA
*Corresponding author. E-mail: bischoa@uni-muenster.de

(Received 13 December 2019; revision accepted 10 March 2020)

Abstract–CM chondrites are complex impact (mostly regolith) breccias, in which lithic clasts show various degrees of aqueous alteration. Here, we investigated the degree of alteration of individual clasts within 19 different CM chondrites and CM-like clasts in three achondrites by chemical analysis of the tochilinite-cronstedtite-intergrowths (TCIs; formerly named "poorly characterized phases"). To identify TCIs in various chondritic lithologies, we used backscattered electron (BSE) overview images of polished thin sections, after which appropriate samples underwent electron microprobe measurements. Thus, 75 lithic clasts were classified. In general, the excellent work and specific criteria of Rubin et al. (2007) were used and considered to classify CM breccias in a similar way as ordinary chondrite breccias (e.g., CM2.2-2.7). In BSE images, TCIs in strongly altered fragments in CM chondrites (CM2.0-CM2.2) appear dark grayish and show a low contrast to the surrounding material (typically clastic matrix), and can be distinguished from TCIs in moderately (CM2.4-CM2.6) or less altered fragments (CM2.7-CM2.9); the latter are bright and have high contrast to the surroundings. We found that an accurate subclassification can be obtained by considering only the "FeO"/SiO_2 ratio of the TCI chemistry. One could also consider the TCIs' S/SiO_2 ratio and the metal abundance, but these were not used for classification due to several disadvantages. Most of the CM chondrites are finds that have suffered terrestrial weathering in hot and cold deserts. Thus, the observed abundance of metal is susceptible to weathering and may not be a reliable indicator of subtype classification. This study proposes an extended classification scheme based on Rubin's scale from subtypes CM2.0-CM2.9 that takes the brecciation into account and includes the minimum to maximum degree of alteration of individual clasts. The range of aqueous alteration in CM chondrites and small spatial scale of mixing of clasts with different alteration histories will be important for interpreting returned samples from the OSIRIS-REx and Hayabusa 2 missions in the future.

INTRODUCTION

Meteorites classified as CI and CM chondrites have the highest degree of aqueous alteration (e.g., Fredriksson and Kerridge 1988; Tomeoka and Buseck 1988; Endress and Bischoff 1993; Johnson and Prinz 1993; Browning et al. 1996; Zolensky et al. 1997, 2002; Bischoff 1998; Brearley 2006; Rubin et al. 2007; Howard et al. 2009; Alexander et al. 2012, 2013; Garenne et al. 2014; Tonui et al. 2014; Visser et al. 2018). Additionally, almost all of these carbonaceous chondrites are heavily brecciated and contain clasts of different mineralogy and chemistry (e.g., Metzler et al. 1992; Bischoff et al. 2006, 2017; Morlok et al. 2006; Lindgren et al. 2013; Zolensky et al. 2015, 2017; Alfing et al. 2019). Some of these rocks even contain fragments that were formed in water-free environments or that have completely lost their volatiles due to heating

(Kerraouch et al. 2018, 2019a, 2019b; Bischoff et al. 2018a; Ebert et al. 2019, 2020).

Since 1963, scientists have studied the secondary phases in CM chondrites that formed by different stages of aqueous alteration. The first discovery of these phases was made by Ramdohr (1963), who described an Fe-C-S mineral. These phases were named "poorly characterized phases" (PCPs) by Fuchs et al. (1973) due to their complex mineralogy. Nowadays, the mineralogy of PCPs is known (e.g., Müller et al. 1979; Mackinnon and Zolensky 1984; Zolensky and McSween 1988): they mainly consist of various serpentine minerals (e.g., cronstedtite) and tochilinite and, therefore, are now called TCIs ("tochilinite-cronstedtite intergrowths"). As TCIs and other secondary phases in CM chondrites formed by different degrees of aqueous alteration (e.g., Fuchs et al. 1973; McSween 1979a; Rubin and Wasson 1986; Grimm and McSween 1989; Brearley [2006] and references therein), different classification schemes for these phases have been proposed to quantify the degree of aqueous alteration of CM chondrites (e.g., McSween 1979b; Browning et al. 1996; Rubin et al. 2007; Howard et al. 2009; Alexander et al. 2012, 2013; Garenne et al. 2014).

One of the first classification schemes using the degree of alteration was developed by McSween (1979b), and it consisted of the three categories (1) partially altered, (2) altered, and (3) highly altered. Rubin et al. (2007) proposed an improved alteration scheme that defined CM2 subtypes by classification of the main lithology based on the abundance and size of the TCIs (former PCPs), the "FeO"/SiO_2 ratio of the TCIs, and the abundances of Ca-carbonates and metals. Since this classification scheme was established, it has been used frequently. Yet, while it does consider well-established, detailed aspects and is easy to understand, it has some major problems:

1. It only considers the degree of aqueous alteration of the major lithology of a thin section. Considering that the exposed specimens used for analysis are often small, 1 inch thin sections, they are not representative in many cases.
2. One of the key observations needed to use this classification scheme is the metal abundance. Unfortunately, because most of the CM chondrites are finds that have suffered weathering in hot and cold deserts (only 18 of 640 CM chondrites are fresh falls; Meteoritical Bulletin Database, December 2019), their original metal abundances cannot be determined. Thus, the observed abundance of metal is susceptible to terrestrial weathering and may not be a reliable indicator of subtype classification.
3. Besides the metal abundance, this classification scheme also incorporates both the calculated S/SiO_2 and "FeO"/SiO_2 ratios for determining the CM-subtype classification. However, the S/SiO_2 ratio may significantly vary in a sample because of the difference in the precursor materials of the TCI alteration product (sulfide versus metal).
4. Most CM chondrites are heavily brecciated (as will be shown below; Fig. 1), and the most abundant lithology can vary from thin section to thin section because the small sections are not representative (see point A above and the following paragraph).

Previous reports have indicated that CM breccias are highly heterogeneous (e.g., Metzler et al. 1992; Bischoff et al. 2006, 2017; Lindgren et al. 2013; Zolensky et al. 2017; Lentfort et al. 2019). For instance, Bischoff et al. (2017) showed that in a single meteorite, the main lithology can vary from one sample to another. Nogoya is an excellent example indicating the heterogeneity of CM breccias in different thin sections; Rubin et al (2007) classified Nogoya as a CM 2.2, whereas the thin section investigated by Bischoff et al. (2017; which is also part of this study) is dominated by a CM2.5 fragment (~70% of the thin section; see Fig. 2). Therefore, Bischoff et al. (2017) proposed an extended classification scheme that gives a range of alteration subtypes (e.g., CM2.2-2.5) for a specific CM chondrite breccia, similar to the classification system used for ordinary chondrites breccias (e.g., H3-5; LL4-6).

During this study, 19 different CM chondrites and three achondrites containing CM-like clasts were examined. They were examined in order (1) to identify the possible brecciation of the sample and (2) to determine the degree of aqueous alteration of individual fragments. TCIs were searched for in 32 polished sections with a scanning electron microscope (SEM) and the help of overview images. Subsequently, 27 thin sections with TCI-bearing fragments/areas were analyzed with the microprobe in order to detect clasts with the highest and lowest alteration types of each sample based on the "FeO"/SiO_2 ratio. For samples with few (no) clearly visible lithologies (Murchison, Santa Cruz, Y-791198, and Maribo), the compositions of the TCIs of the main lithology (bulk rock) were obtained.

Our classification procedure for individual clasts mainly considers the "FeO"/SiO_2 ratios mentioned by Rubin et al. (2007) to make distinctions between several CM subtypes, as we have done in earlier studies (Bischoff et al. 2017; Lentfort et al. 2019). Thus, we classify CM chondrites based on the constituents of different clasts, as is done for ordinary chondrite breccias (e.g., Bischoff et al. 2006, 2018b; Metzler et al. 2011). The classification scheme of Rubin et al. (2007) is limited to subtypes not higher

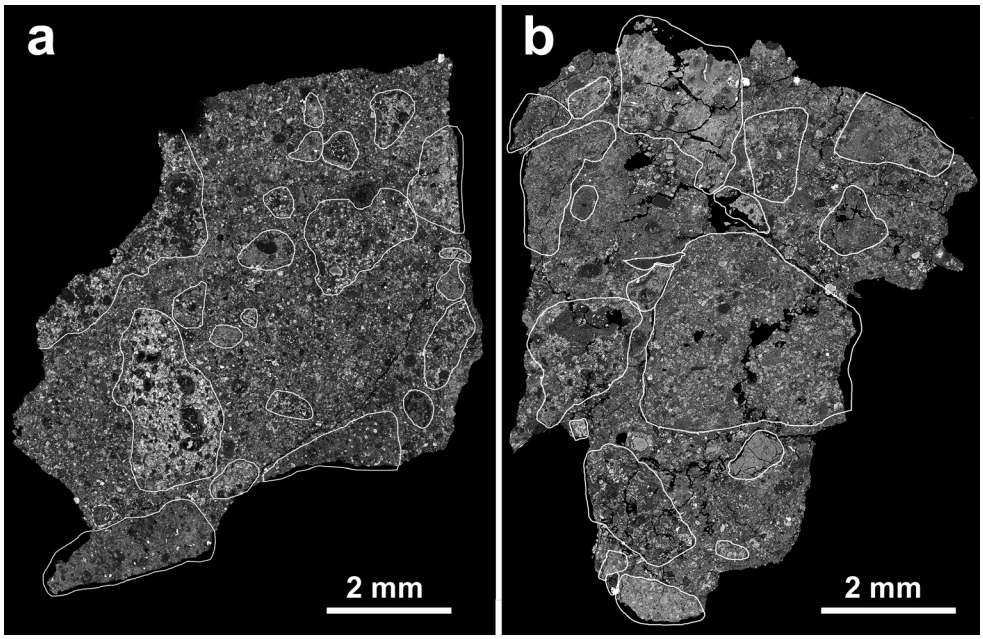

Fig. 1. CM breccias ALH 85013 (a) and LON 94101 (sample: co. 36) (b). Fragments showing different degrees of alteration are embedded in a fine-grained clastic matrix. Images in backscattered electrons.

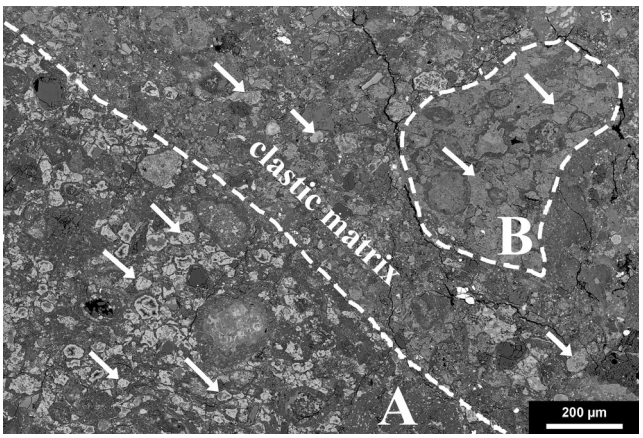

Fig. 2. Fragment A with subtype CM2.5 and fragment B with subtype CM2.2 of Nogoya. The TCIs of fragment A show a light gray appearance (bright, arrows) and high contrast to the surrounding clastic matrix. Fragment B contains darker grayish TCIs (arrows) and shows less contrast to the surrounding material. BSE image.

than 2.6, though subsequent work suggested that the Paris CM chondrite has subtype of at least 2.7 (Rubin 2015). In this study, we use ratios of "FeO"/SiO_2 to define criteria for CM 2.7, 2.8, and 2.9 subtypes to help compare weakly altered CM chondrites. Finally, we compare our classification results with those of Rubin et al. (2007).

SAMPLES AND ANALYTICAL METHODS

Samples

Thirty-two thin sections of 19 different CM chondrites (including the anomalous CM chondrites WIS 91600, Dhofar 225, and NWA 10907/10908) and CM fragments in three achondrites were investigated. Table 1 lists all investigated CM chondrites and achondrites having CM-like fragments, whether they are falls or finds, the country of discovery, their type, the source of the sample, and the number of investigated samples for SEM and/or EMP studies.

For most of the samples, distinct fragments were analyzed. A fragment is defined as an area that contains TCIs and can be clearly distinguished from the components within the surrounding material, which is the typical clastic matrix of a CM breccia (e.g., Fig. 1). For the few samples with optically unclear identification of distinct clasts of different degrees of aqueous alteration, the TCIs of the entire samples were randomly analyzed.

The anomalous and untypical CM samples (WIS 91600, Dhofar 225, and NWA 10907/10908) were removed from the main study and are described in Supplement S1 in supporting information. The same holds for some fragments in CM chondrite breccias. Two examples are shown in Fig. 3, and more fragments are shown in Supplement S1.

Table 1. List of investigated samples.

Name	Abbreviation	Fall or find	Location/country	Type (old classification)	Source	Thin section
Allan Hills 85013	ALH 85013	Find	Antarctica	CM2	NASA-JSC[a]	1 pts
Alan Hills A 77306	ALHA 77306	Find	Antarctica	CM2	NASA-JSC[a]	1 pts
Lonewolf Nunataks 94101	LON 94101	Find	Antarctica	CM2	NASA-JSC[a]	6 pts[b]
Queen Alexandra Range 94582	QUE 94582	Find	Antarctica	CM2	NASA-JSC[a]	1 pts
Santa Cruz		Fall	Tamaulipas, Mexico	CM2	NASA-JSC[a]	2 pts (1 and 3)
Wisconsin Range 91600	WIS 91600	Find	Antarctica	CM2	NASA-JSC[a]	2 (19 and 20)
Banten		Fall	Jawa Barat, Indonesia	CM2	Münster	PL93094 (1) PL95111 (2)
Cold Bokkeveld		Fall	Western Cape, South Africa	CM2	Münster	PL17148 (A) PL98139 (B)
Dhofar 225	Dho 225	Find	Zufar, Oman	CM-an	Münster	PL09087
Dhofar 735	Dho 735	Find	Zufar, Oman	CM2	Münster	PL09088
Jbilet Winselwan		Find	Saguia el Hamra, Western Sahara	CM2	Münster	PL13070
Maribo		Fall	Region Sjaelland, Denmark	CM2	Münster	PL09089
Northwest Africa 12651	NWA 12651	Find	Morocco	CM	Münster	PL17261
Murchison		Fall	Victoria, Australia	CM2	Münster	PL89463
Nogoya		Fall	Entre Rios, Argentina	CM2	Münster	PL13060
Northwest Africa 10907	NWA 10907	Find	Morocco	CM2	Münster	PL17075
Northwest Africa 10908	NWA 10908	Find	Morocco	CM2	Münster	PL17076
Northwest Africa 11086	NWA 11086	Find	Morocco	CM-an	Münster	PL17251
Yamato 791198	Y-791198	Find	Antarctica	CM2	Münster/ NIPR	PL98140
Elephant Moraine 87513	EET 87513	Find	Antarctica	Howardite	NASA-JSC[a]	EET87513,13
Northwest Africa 7542	NWA 7542	Find	(Northwest Africa)	Eucrite-pmict	Münster	PL14058 (A) PL14058 (B)
Sariçiçek		Fall	Bingol, Turkey	Howardite	Münster	PL16014

[a]Provided by Mike Zolensky (NASA Johnson Space Center, Houston).
[b]Includes the sample names: MZ1, MZ2, Cari 6, co,34, co. 36 and 34.

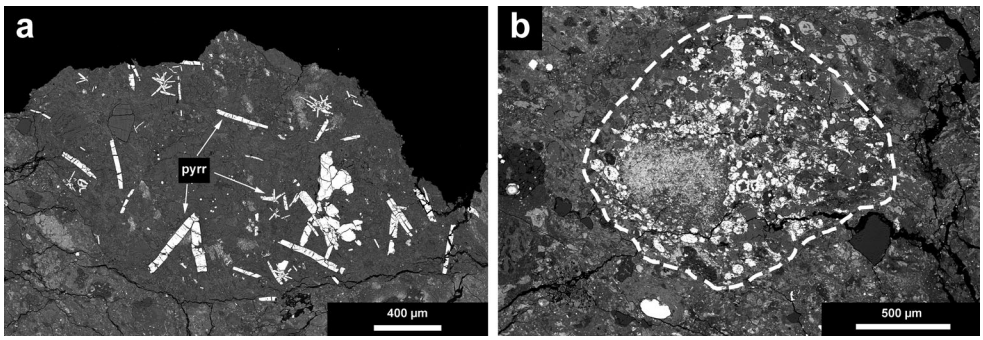

Fig. 3. Examples of two fragments from LON 94101 that do not represent typical CM lithologies. a) C1-related clast with abundant pyrrhotite laths (pyrr); (b) clast that looks like it contains bright TCIs. However, the analyses show that these objects contain abundant sulfide- or metal-related components and, therefore, are not "real" TCIs. BSE images.

Scanning Electron Microscopy

A JEOL JSM-6610LV SEM at the Interdisciplinary Center for Electron Microscopy and Microanalysis at the Westfälische Wilhelms-Universität Münster operating at 20 kV was used to image whole samples and areas of interest. Overview images were assembled using the Microsoft image composition editor. These images were used to search for and to register fragments with different degrees of alteration for further studies (e.g., microprobe analysis). Since CM chondrites occur as fragments in other polymict meteorites, CM-like fragments in three achondrites were also investigated.

The SEM was also used for quantitative EDS analysis of some TCIs within Y-791198 by rastering appropriate areas. For TCI analyses, different natural and synthetic Astimex standards were used: olivine (Mg, Fe, Si), jadeite (Na), plagioclase (Al), sanidine (K), diopside (Ca), rutile (Ti), chromium oxide (Cr), rhodonite (Mn), pentlandite (Ni, S), and apatite (P). For EDS analyses, the INCA analytical program provided by Oxford Instruments was used.

Electron Microprobe Analysis

Quantitative TCI analyses of different fragments and measurements of phyllosilicates of the host unit were obtained using a JEOL JXA-8530F field emission electron microprobe at the Institut für Mineralogie (Münster), which was operating at 15 kV and with a probe current of 15 nA. For TCI and phyllosilicate analyses, different natural and synthetic standards were used: Na (jadeite), Mg (San Carlos olivine), Al (disthene), Si (hypersthene), P (apatite), S (celestine), K (sanidine), Ca (diopside), Ti (rutile), Fe (fayalite), Cr (Cr_2O_3), Mn (rhodonite), Ni (NiO), and Cl (tugtupite). The measuring points were distributed on the TCIs with variable spot sizes between 3 and 15 µm depending on the size of the TCI (Fig. 4). Some fragments with coarse-grained or fishbone-like TCIs (e.g., in Maribo) were measured with larger spot sizes up to 30 µm. The analyses of TCIs of the host unit for samples with few/no fragments were done with variable spot sizes between 10 and 30 µm. Examples for the selection of analyzed TCIs in specific fragments are given in Fig. 4.

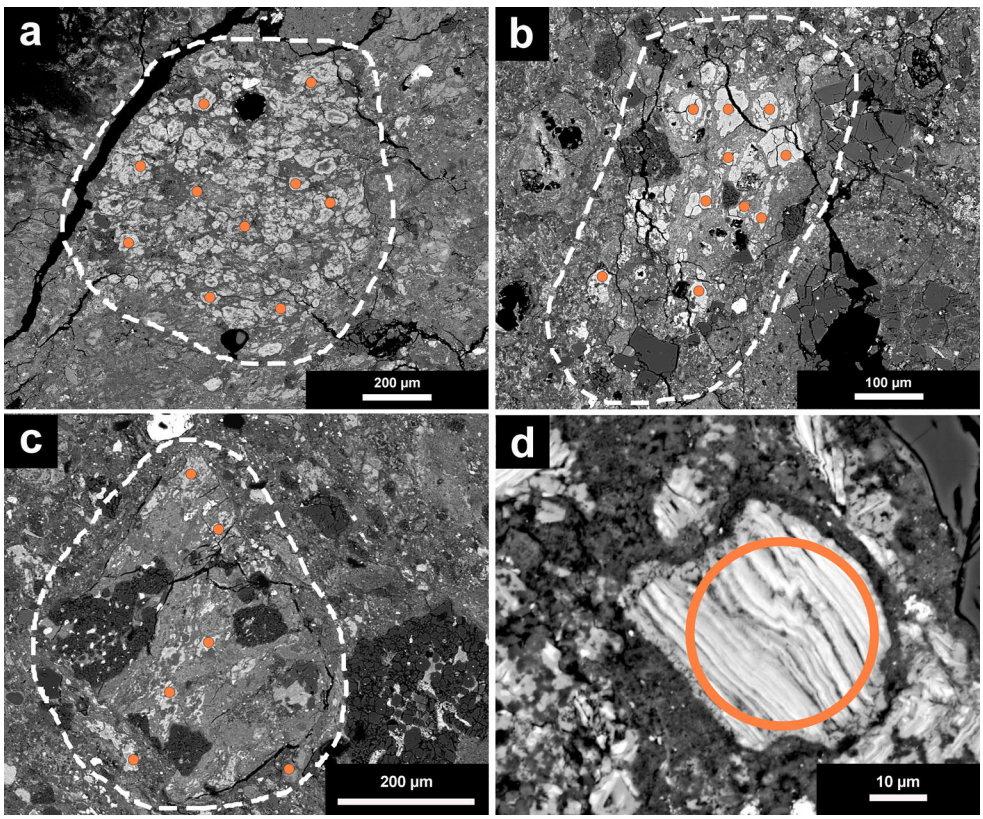

Fig. 4. Fragments within CM breccias with the illustration of spots of analysis on TCIs: (a) LON 94101 (thin section: co. 34; fragment D; subtype CM2.4); (b) Jbilet Winselwan (fragment B; CM2.9); (c) Banten 2 fragment B (subtype CM2.8); (d) Maribo coarse-grained TCIs (subtype CM2.6). Please note that the dashed lines do not exactly correspond to the boundaries of the clasts. BSE images.

Considering the results given in Table 2, the "FeO" value is given with quotation marks because it is not clear which form of Fe was measured; the measurements could include variable abundances of FeO in phyllosilicates, Fe^{2+} in sulfides, and Fe^{3+} in cronstedtite (compare with Rubin et al. 2007). A small number of measurements were excluded from the average calculation of the TCI compositions because of contamination with surrounding phases. This includes measurements with >3.0 wt% Ni (perhaps from pentlandite or metal) and CaO> 3.0 wt% (probably due to abundant calcite). Most analyses show SiO_2 values of > 10.0 wt%, similar to those of Rubin et al. (2007). Three samples show lower than 10 wt% SiO_2, but these samples fit into the trend indicating a higher subtype classification.

In the past, the calculated S/SiO_2 and "FeO"/SiO_2 ratios and the metal abundance were mainly considered for the CM2 subtype classifications (compare tables 4 and 5 of Rubin et al. 2007). Although the "FeO"/SiO_2 ratios play a key role in the subtype classification by Rubin et al. (2007), that classification system also uses the other characteristics. In this study, we will only use the "FeO"/SiO_2 ratios. The results of the analyses of 1000 TCIs in distinct clasts and bulk meteorites are given in Table 2.

RESULTS

Investigated Meteorites

Nineteen different CM chondrites and various CM-like clasts in three achondrites were examined. Most samples are characterized by clear evidence of being polymict breccias (Figs. 1–5); however, the degree of brecciation can be highly variable on a thin section (cm) scale. Murchison, Santa Cruz, Y-791198, and Maribo only show very weak or unclear evidence of brecciation, and the degree of aqueous alteration was obtained by random analyses of TCIs in several areas of the bulk sample (Table 2).

Chemical Composition of TCI-Rich Fragments within CM Chondrites

From the different meteorites, 27 thin sections were chosen for microprobe analysis to subclassify the fragments within the CM chondrites (and brecciated achondrites) or for random TCI analysis in the case of the widely unbrecciated rocks (Table 2). Some fragments that optically appear to be TCI-rich fragments turned out not to be, but rather contain metal- or sulfide-rich intergrowths (Fig. 3b; see Supplement S1). Those and other fragments were excluded from the subtype classification (see Supplement S1).

Most of the investigated fragments and the unbrecciated bulk rocks can be classified according to the classification scheme of Rubin et al. (2007), mainly based on the "FeO"/SiO_2 ratio. The "FeO"/SiO_2 ratio decreases as alteration increases (Table 2; Fig. 6). Some clasts show significantly higher "FeO"/SiO_2 ratios than the highest mentioned by Rubin et al. (2007) for the subtype classification of 2.6 ("FeO"/SiO_2 ratio >3.3). Therefore, in this work, we defined new threshold values for subtypes CM2.7-2.9. The "FeO"/SiO_2 values for the borders are related to data from Rubin et al. (2007), who defined the borders of CM2.2/2.3 (at 1.5 and 1.7, mean of 1.6 used here), CM2.4/2.5 (at 2.0), and CM2.6/2.7 (at 3.3) in their table 5. All threshold values for the subgroups CM2.0-CM2.9 used in this work are given in Table 3. Based on these values, the classified subtypes for the different fragments and bulk rocks (or main lithologies, if some fragments may occur) of all investigated samples are listed in Table 2.

In general, a positive correlation is observed when the "FeO"/SiO_2 ratios of the analyzed TCIs in the individual clasts are plotted against the S/SiO_2 ratios (Fig. 6). However, there are deviations from the trend: Remarkable exceptions of the positive correlation are shown by the values obtained for several clasts (especially for fragment B of Jbilet Winselwan, fragment C of LON 94101 co. 34, both fragments [A and B] of NWA 12651, and some others; see the large triangle in Fig. 6). These fragments show low S/SiO_2 ratios compared to relatively high "FeO"/SiO_2 ratios and, therefore, do not fit into the correlation. These fragments will be considered in detail in the discussion.

The mean compositions of some main oxides (SiO_2, "FeO," MgO) and ratios of all subtypes (CM2.0-CM2.9) are given in Table 3. The single subtypes generally show smooth transitions. In some cases, values slightly overlap, and a clear distinction is only possible by using the "FeO"/SiO_2 ratio. The mean "FeO"/SiO_2 and S/SiO_2 ratios as well as the "FeO" content increase from strongly altered to moderately or less altered subtypes, while the mean MgO and SiO_2 concentrations decrease from strongly altered to less altered samples (Table 3). Therefore, other correlations are obvious when considering the different aqueous alteration subtypes (Fig. 7). Figure 7 shows a negative correlation between the "FeO"/SiO_2 ratio and the MgO content (wt%). Strongly altered subtypes (2.0–2.2) have higher MgO contents of ~15.0–27.0 wt% compared to moderately or weakly altered subtypes (>2.6), with MgO concentrations of ~5.0 to 10.0 wt%. Furthermore, the abundance of clearly visible and weakly altered components (such as chondrules) increases with higher subtype classification. Table 3 also includes some additional aspects concerning

Table 2. Mean S/SiO_2 and "FeO"/SiO_2 ratios of the studied fragments and of TCI measurements of the main lithology for samples with very few fragments (Murchison, Y-791198, Jbilet Winselwan). For samples with no clearly detectable fragments (Santa Cruz, Maribo), the TCIs of the bulk rock were randomly analyzed. Subtype classification of fragments/areas only based on the mean values of the "FeO"/SiO_2 ratio; fragments within individual polished sections are ordered based on the "FeO"/SiO_2 ratio.

Meteorite	Subsample	Fragment (n)	S/SiO_2 ratio	"FeO"/SiO_2 ratio	Subtype
LON 94101	MZ1	E (9)	0.15	0.89	2.0
		B (11)	0.22	1.57	2.2
		G (4)	0.28	1.83	2.4
		C (9)	0.55	2.95	2.6
		A (19)	0.45	2.40	2.5
		D (15)	0.83	4.18	2.8
LON 94101	MZ2	C (8)	0.06	0.61	2.0
		D (4)	0.18	1.27	2.2
		F (4)	0.13	1.80	2.4
		B (5)	0.12	1.85	2.4
		A (8)	0.55	3.09	2.6
		E (5)	0.22	3.35	2.7
LON 94101	Cari 6	A (13)	0.11	1.46	2.2
		B (14)	0.14	1.56	2.2
LON 94101	co. 34	D (10)	0.35	1.84	2.4
		B (7)	0.24	2.35	2.5
		C (9)	0.06	3.27	2.6
		A (10)	0.51	3.47	2.7
LON 94101	co. 36	E (5)	0.14	0.83	2.0
		G (6)	0.16	1.23	2.2
		A (8)	0.18	1.52	2.2
		B (5)	0.27	1.82	2.4
		D (12)	0.25	1.83	2.4
		F (5)	0.25	1.88	2.4
		C (5)	0.44	2.68	2.5
ALH 85013		C (6)	0.21	1.57	2.2
		A (14)	0.35	2.09	2.5
		D (4)	0.11	2.85	2.6
		B (12)	0.74	3.41	2.7
		F (12)	0.23	3.84	2.7
ALHA 77306		G (5)	0.04	0.73	2.0
		C (6)	0.17	2.04	2.5
		F (5)	0.11	2.08	2.5
		A (12)	0.17	2.14	2.5
		B (6)	0.26	2.32	2.5
		D (7)	0.33	2.96	2.6
Murchison		Main lithology (51)	0.61	4.01	2.7
		A (5)	0.74	5.04	2.9
		C (4)	0.75	5.58	2.9
		B (14)	0.98	5.92	2.9
Banten	1	A (13)	0.30	3.05	2.6
		C (11)	0.40	3.62	2.7
		D (6)	0.60	5.57	2.9
		B (4)	0.87	6.92	2.9
Banten	2	C (5)	0.21	3.77	2.7
		D (8)	0.51	3.82	2.7
		A (8)	0.52	3.92	2.7
		B (7)	0.36	4.72	2.8
		E (5)	0.71	5.12	2.9

Table 2. *Continued*. Mean S/SiO_2 and "FeO"/SiO_2 ratios of the studied fragments and of TCI measurements of the main lithology for samples with very few fragments (Murchison, Y-791198, Jbilet Winselwan). For samples with no clearly detectable fragments (Santa Cruz, Maribo), the TCIs of the bulk rock were randomly analyzed. Subtype classification of fragments/areas only based on the mean values of the "FeO"/SiO_2 ratio; fragments within individual polished sections are ordered based on the "FeO"/SiO_2 ratio.

Meteorite	Subsample	Fragment (n)	S/SiO_2 ratio	"FeO"/SiO_2 ratio	Subtype
*Y-791198		Main lithology (66)	0.37	2.95	2.6
		A (5)	0.67	4.31	2.8
Maribo		Bulk rock (110)	0.32	3.07	2.6
Jbilet Winselwan		C (8)	0.05	1.99	2.4
		Main lithology (32)	0.08	2.52	2.5
		B (9)	0.06	6.15	2.9
NWA 12651		B (17)	0.02	4.08	2.7
		A (15)	0.02	4.33	2.8
Cold Bokkeveld	A	G (7)	0.23	1.56	2.2
		C (20)	0.17	1.63	2.3
		F (19)	0.20	1.93	2.4
		B (13)	0.21	1.95	2.4
		D (15)	0.27	2.18	2.5
		E (17)	0.31	2.50	2.5
		A (10)	0.44	3.60	2.7
Cold Bokkeveld	B	E (7)	0.12	1.18	2.1
		D (7)	0.12	1.77	2.4
		B (19)	0.08	1.80	2.4
		A (15)	0.24	1.92	2.4
		C (11)	0.37	2.49	2.5
Nogoya		B (11)	0.12	1.31	2.2
		C (5)	0.19	2.12	2.5
		A (21)	0.21	2.28	2.5
Santa Cruz	1	Bulk rock (49)	0.28	3.62	2.7
CM-fragments in HED-meteorites					
NWA 7542	A	10 (7)	0.04	1.53	2.2
		16 (6)	0.13	2.45	2.5
		18 (5)	0.31	3.00	2.6
NWA 7542	B	13 (10)	0.3	2.96	2.6
		14 (8)	0.31	3.11	2.6
		11 (9)	0.34	4.49	2.8
EET 87513	,13	02 (7)	0.19	2.76	2.6

n = number of analyses.
*SEM measurements.

the optical appearance of the TCIs and their visible contrast to the surrounding materials.

Chemical Composition of TCIs in CM chondrites without Clearly Detectable Fragments

For some samples with few or no obvious fragments, the compositions of the TCIs of the host unit were measured. The S/SiO_2 ratio, "FeO"/SiO_2 ratio, and subtype of the TCI measurements from the host units are given in Table 2. In Maribo and Santa Cruz, no distinct fragment could be identified; thus, the composition of the TCIs of the bulk rock was determined. In Yamato 791198 Murchison, and Jbilet Winselwan, very few barely visible fragments were observed from which the compositions of the TCIs were obtained. Most samples, especially those from Murchison, show high "FeO"/SiO_2 ratios, indicating a low degree of alteration (Table 3). Besides these fragments, the compositions of the TCIs of the remaining main lithology were obtained by random analyses of TCIs. Figure 8 shows the "FeO"/SiO_2 versus S/SiO_2 ratio for TCIs in the bulk rock (in the case of Maribo and Santa Cruz) or the main lithology of these CM chondrites.

The positive correlation between the "FeO"/SiO_2 and S/SiO_2 ratio is visible in the diagram. It is

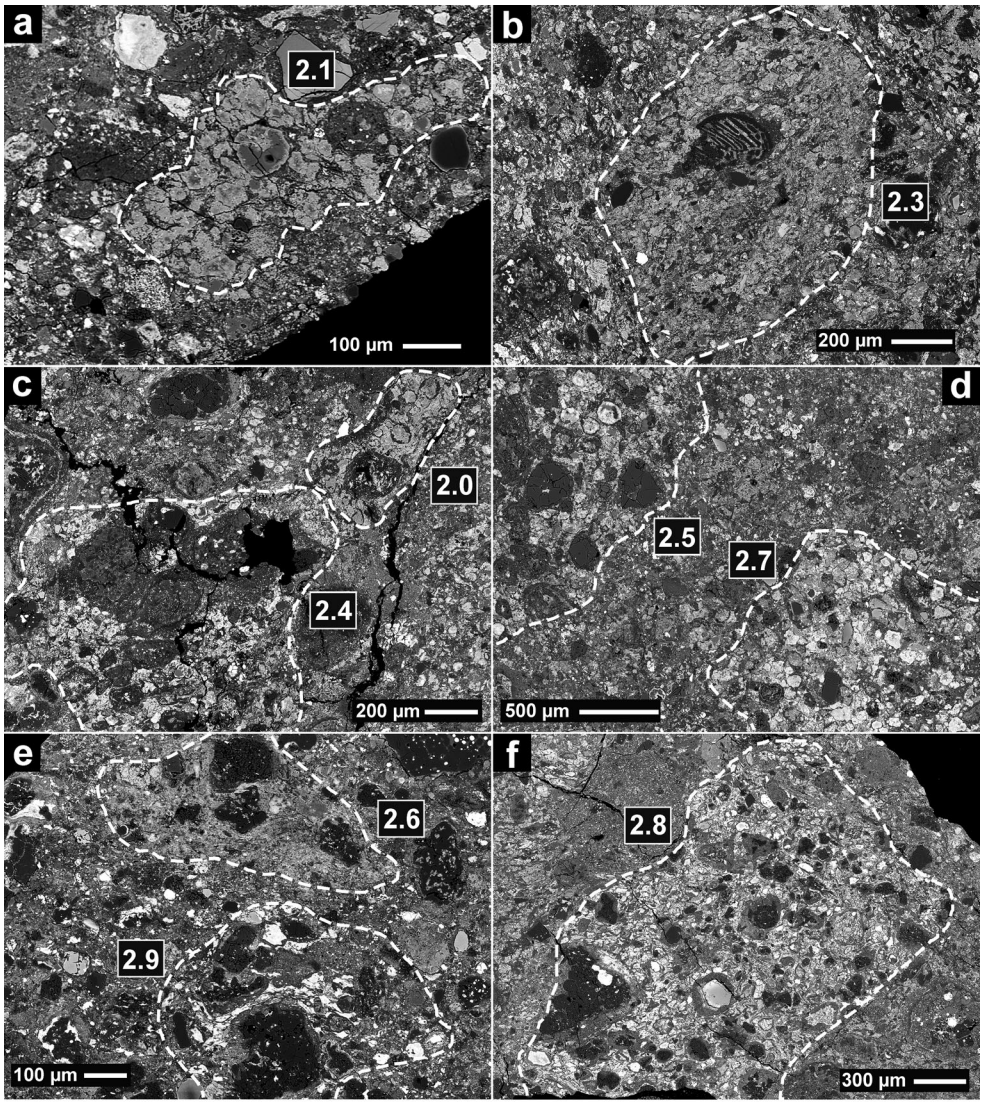

Fig. 5. BSE images of various clasts with different petrological subtypes. a) Cold Bokkeveld B—clast E; type CM2.1. b) Cold Bokkeveld A—clast C; type CM2.3. c) LON 94101 co.36—clast E; type CM2.0 and clast D; type CM2.4. d) ALH 85013 clast A; type CM2.5 and clast B; type CM2.7. e) Banten—clast A; type CM2.6 and clast B; type CM2.9. f) LON 94101 MZ1—clast D; type CM2.8.

noticeable that the TCI measurements of the main lithologies (host unit) of Jbilet Winselwan and Santa Cruz also do not completely fit in the trend because of a low S/SiO_2 ratio in comparison to a relatively high "FeO"/SiO_2 ratio. Since only the "FeO"/SiO_2 ratio is used in this work, these rocks have to be classified as CM2.5 and 2.7, respectively.

Fragments Having TCIs with Low S/SiO_2 Ratios

Considering all analyzed fragments in the studied CM breccias, some clasts can be characterized by having low concentrations of sulfur, resulting in very low S/SiO_2 ratios compared to the "FeO"/SiO_2 ratios (Table 4). These special clasts can be identified in the triangle of Fig. 6.

CM-Like Fragments in Achondrites

CM-like clasts can be frequently observed in polymict eucrites, howardites, and rarely in H chondrites (e.g., Fodor and Keil 1976; Zolensky et al. 1996; Gounelle et al. 2003; Patzek et al. 2018a). Previously, we identified and characterized a large number of CM-like clasts (>60) in 15 different HEDs together with CI-like clasts in HEDs and other achondrite and chondrite groups (Patzek et al. 2018a). Based on this survey, we selected seven clasts for which we here aimed to determine the petrologic subtypes (Table 2). Three of these clasts observed in the polymict breccias NWA 7542 and EET 87513 are shown in Fig. 9. While clast

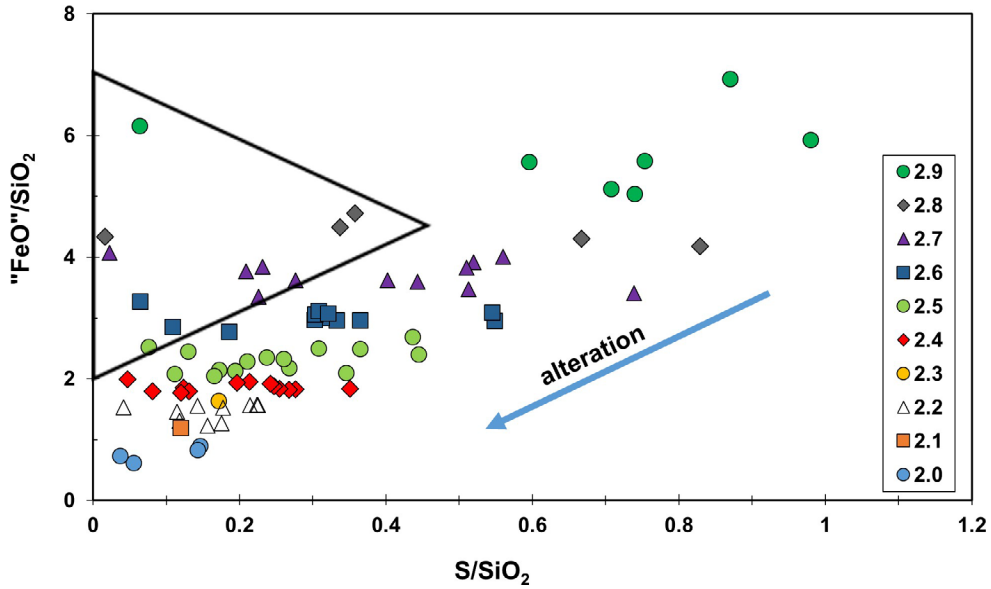

Fig. 6. "FeO"/SiO_2 versus S/SiO_2 ratios of TCIs for aqueous alteration types of all fragments/areas (bulk rocks, main lithologies) with subtypes from 2.0 to 2.9. The samples in the triangle are discussed in detail in the text.

NWA 7542A-10 turned out to be of petrologic subtype 2.2, the clasts NWA 7542B-13 and EET 87513-02 are of petrologic type 2.6 (Fig. 9). This CM classification is in agreement with results on the abundance and appearance of individual chondrules and TCI lumps that are surrounded by fine-grained rims (Metzler et al. 1992; Metzler and Bischoff 1996). EET 87513-02 contains abundant chondrules as well as fragments of Fo-rich and En-rich olivine and pyroxene, which are embedded in a mixture of TCI lumps and fine-grained clastic matrix (e.g., Fig. 9c). Several sulfides including pyrrhotite (sometimes close to stoichiometric FeS), pentlandite, and a P-rich sulfide can be observed when viewed in detail. Additionally, a heavily fractured CAI can be observed in one of the clasts that consists of spinel and Ca-rich pyroxene and shows incipient aqueous alteration at the rims. Additionally, several of the unshocked or very weakly shocked clasts consist of different lithologies, themselves resembling the brecciated nature of common CM2 chondrites (Fig. 9b).

DISCUSSION

Optical and Chemical Characteristics of Individual Fragments

The investigation of different CM chondrites shows that TCI-rich fragments with different aqueous alteration stages can be distinguished using "FeO"/SiO_2 of TCIs and BSE contrast between TCIs and surrounding matrix.

Strongly altered and less altered TCI-rich fragments can be optically distinguished by differences in brightness of the TCIs in BSE images, which, in most cases, contrast with the surrounding clastic matrix. In detail, strongly altered TCI-rich fragments (CM2.0-2.3) appear dark-grayish and generally only show a low contrast to the surrounding material (Figs. 2 and 5a, 5b, 5c), whereas the moderately altered TCI-rich fragments (CM2.4-2.6) show a brighter appearance on BSE images compared to the surrounding matrix (Figs. 2 and 4a). Less altered TCI-rich fragments (CM2.7-2.9) show the brightest appearance and have the highest contrast to the surrounding material (Figs. 4b and 5d, 5e, 5f).

The occurrence of chondrules or other inclusions (CAIs, fragments) can also reflect the degree of aqueous alteration. Strongly altered fragments typically contain components with a high degree of alteration. In these cases, the phenocrysts within chondrules are often replaced by phyllosilicates, whereas the less altered fragments contain a higher abundance of unaltered and minimally altered coarse-grained components (i.e., chondrules, CAIs, and fragments).

As also noted by Rubin et al. (2007), the metal content of different subtypes can also reflect the degree of aqueous alteration. Typically, clasts with a low degree of alteration have a higher abundance of metals. However, the metal abundance is difficult to estimate, since the metal grains are often very small and are

Table 3. Appearance in BSE images and mean concentrations of selected elements (wt%) of TCIs in different subtypes of aqueously altered CM fragments. The "FeO"/SiO_2 values for the borders (threshold values) are related to data of Rubin et al. (2007), who defined the borders for CM2.2/2.3 (at 1.5 and 1.7, mean of 1.6 used here), for CM2.4/2.5 (at 2.0), and for CM2.6/2.7 (at 3.3) in their table 5. For the main lithology of Paris, Rubin (2015) found a high "FeO"/SiO_2 value and suggested that a CM2.7 should have an "FeO"/SiO_2 value between 4.0 and 7.0, which would be a CM2.8 or CM2.9 in this study.

	2.0 (n = 4)		2.1 (n = 1)		2.2 (n = 10)		2.3 (n = 1)		2.4 (n = 14)		2.5 (n = 15)		2.6 (n = 12)		2.7 (n = 12)		2.8 (n = 5)		2.9 (n = 7)	
Subtype	Mean	SD	Mean	SD	Mean	SD	Mean	SD	Mean	SD	Mean	SD	Mean	SD	Mean	SD	Mean	SD	Mean	SD
Optical appearance	Dark gray		Dark gray		Dark gray/ gray		Gray		Gray		Gray		Light gray		Light gray		Light gray		Brightest appearance	
Contrast to surroundings	Low contrast		Low contrast		Low contrast		Moderate contrast		Moderate contrast		Moderate contrast		Moderate contrast		High contrast		High contrast		High contrast	
SiO_2	30.0	2.8	26.0	–	23.7	1.6	21.8	–	21.1	1.3	18.5	1.4	16.5	1.3	14.4	1.3	13.3	1.1	9.6	1.1
FeO	22.2	2.1	30.6	–	34.1	2.9	35.4	–	38.5	3.2	41.3	2.5	48.0	3.3	49.8	5.6	53.7	5.5	53.6	5.0
MgO	24.9	1.0	17.2	–	16.7	2.1	14.5	–	13.9	2.1	12.2	1.5	9.7	2.8	8.2	2.6	7.5	2.7	5.6	0.9
S/SiO_2	0.10	0.06	0.12	–	0.16	0.06	0.17	–	0.20	0.09	0.25	0.11	0.31	0.15	0.39	0.20	0.44	0.32	0.67	0.30
"FeO"/SiO_2	0.76	0.12	1.18	–	1.46	0.14	1.63	–	1.86	0.07	2.31	0.20	3.00	0.13	3.71	0.23	4.41	0.21	5.76	0.65
Threshold value	<0.9		>0.9		>1.2		>1.6		>1.8		>2.0		>2.7		>3.3		>4.1		>4.9	

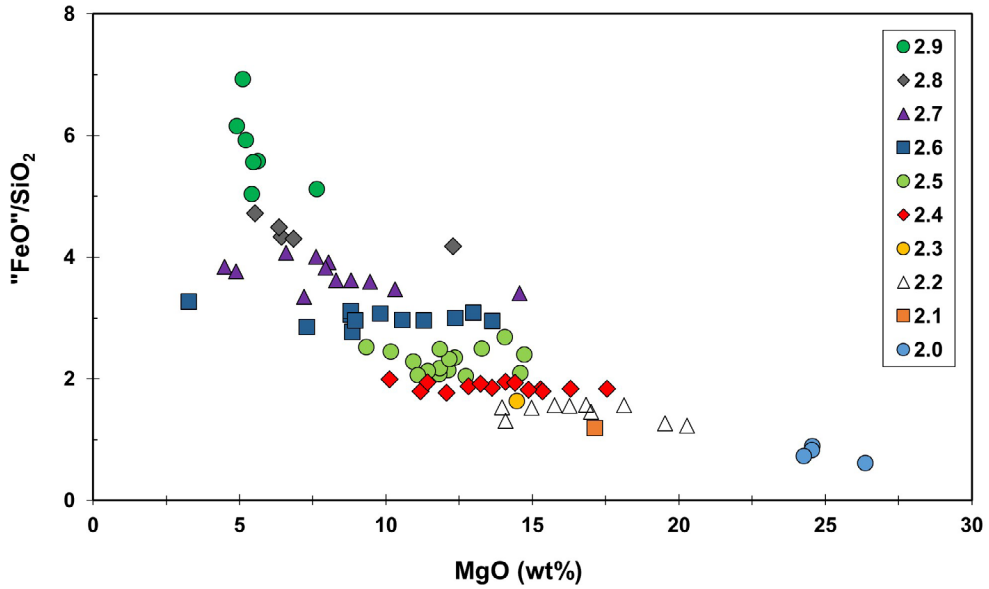

Fig. 7. "FeO"/SiO_2 versus MgO concentration (in wt%) of TCIs for clasts with different aqueous alteration subtypes in CM breccias (compare Tables 2 and 3). Whereas the "FeO/SiO_2" value of different subtypes can be clearly distinguished, the MgO concentration of different subtypes overlaps with those of the adjacent subtypes implying that the "FeO/SiO_2" value is more useful.

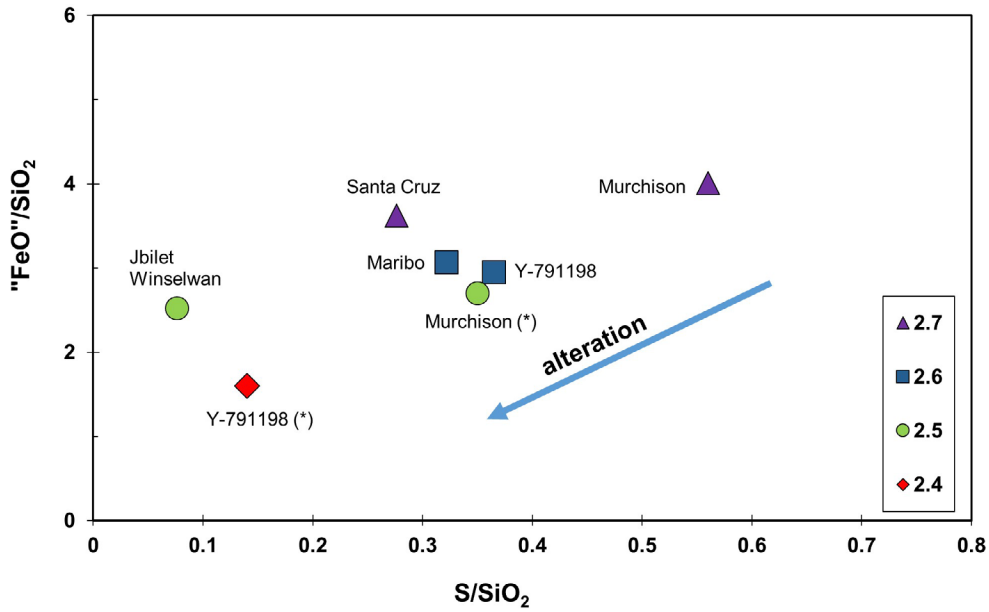

Fig. 8. "FeO"/SiO_2 versus S/SiO_2 ratios of TCIs from samples with few or no clearly defined TCI-rich fragments (main lithology or bulk rock, respectively; Table 2). Murchison clearly shows the lowest degree of alteration. (*) TCI compositions from Rubin et al. (2007).

affected by terrestrial weathering resulting in the oxidation of metal grains. The tendency that strongly altered fragments contain no/few metals and moderately and less altered fragments contain more metals can often be observed if fresh meteorite falls are considered. A good example is the Nogoya breccia, in which the strongly altered fragment B (CM2.2) contains no metal, and the moderately altered fragment A (CM2.5), which contains some metals. Nonetheless, using the metal abundance for subgroup classification of most CM chondrites is inappropriate because less than 3% of CM chondrites represent fresh meteorite falls.

Table 4. Chemical characteristics and subtype classification of selected fragments with low S contents in TCIs. Sulfur concentrations in wt%.

Sample	Fragment	S	S/SiO_2 ratio	"FeO"/SiO_2" ratio	Subtype
LON 94101 MZ2	E	3.60	0.23	3.35	2.7
LON 94101 co. 34	C	1.07	0.07	3.27	2.6
ALH 85013	D	1.84	0.11	2.85	2.6
	F	3.50	0.23	3.84	2.7
Banten 2	B	4.30	0.36	4.72	2.8
	C	2.93	0.21	3.77	2.7
Jbilet Winselwan	B	0.53	0.06	6.15	2.9
NWA 12651	A	0.23	0.02	4.33	2.8
	B	0.39	0.02	4.08	2.7
NWA 7542-B	11	4.05	0.34	4.49	2.8

The optical characteristics observed in BSE images are certainly related to chemical parameters, especially the "FeO" concentrations of the TCIs within the fragments. The FeO, SiO_2, and MgO concentrations as well as the "FeO"/SiO_2 and S/SiO_2 ratios indicate distinct chemical trends related to the degree of aqueous alteration (Figs. 7 and 8). In general—as was also found by Rubin et al (2007)—the MgO and SiO_2 contents decrease from strongly altered to moderately altered and less altered samples (Table 3). The mean SiO_2 content of strongly altered samples (subtype CM2.0) is ~30 wt%, while moderately altered (subtype CM2.4) and less altered fragments (CM2.9) have concentrations of ~21 and ~10 wt%, respectively. Also, the mean MgO concentration decreases from ~25 wt% (subtype CM2.0) to ~5.5 wt% (CM2.9). The mean FeO content for subtype CM2.0 increases from ~22 wt% to ~53.5 wt% (CM2.9). Consequently, the "FeO"/SiO_2 ratio increases from 0.76 for CM2.0 up to 5.76 for subtype CM2.9 and, appropriately, the S/SiO_2 ratio from 0.10 to 0.67. For most of the investigated TCI-rich fragments and CM bulk rocks (or main lithologies; Table 2), the classification scheme of Rubin et al. (2007) works well. However, some TCI-rich fragments of higher subtypes (CM >2.5) have lower S/SiO_2 ratios, which does not fit this trend (Fig. 6).

Variable S Concentrations Among Individual Clasts

As mentioned above, some TCI-rich fragments of high subtypes (CM> 2.5) have too low S/SiO_2 ratios to fit this trend (Fig. 6). Fragments with low S/SiO_2 ratios are: LON 94101 co. 34 fragment C, Jbilet Winselwan fragment B, 12651 fragment A and B, LON 94101 MZ2 fragment E, ALH 85013 fragment D and F, Banten 2 fragment B and C, Santa Cruz 1 fragment A1 and B, and NWA 7542-B fragment 11. These fragments show low S/SiO_2 ratios relative to their high "FeO"/SiO_2 ratios. The sulfur depletions could have arisen for at least two different reasons (1) the precursor materials from which the TCIs formed contained less S or (2) the S may have been redistributed (washed out) during aqueous alteration on the meteorite parent body.

Regarding the first reason, if we consider that typical TCI compositions include abundant Fe and S, this may indicate that the TCIs were formed from precursors containing sulfides such as troilite, pentlandite, or pyrrhotite. Thus, the precursor material for the S-depleted TCIs could have been a metal-rich component. As a result, the TCIs would show low S concentrations compared to Fe. This could explain the greater variety in S content for different TCI-rich fragments. However, this cannot explain why fragments of higher subtypes generally contain more S than fragments with lower subtypes (CM2.0-CM2.4).

The second possibility, that S was redistributed during the aqueous alteration (Fig. 6), can explain this observation much better. This process would generally lead to lower S abundances in fragments suffering from a higher degree of aqueous alteration. However, for the S-depleted fragments having a high petrologic subtype (CM> 2.5), these TCIs may have formed from precursor materials depleted in S-bearing phases such as metals.

TCI Compositions within Rocks with a Low Abundance of or without Distinguishable Clasts

As described above, no distinct fragments could be identified in Maribo and Santa Cruz; thus, the composition of the TCIs from the bulk rock was determined (Table 2; Fig. 10). In Yamato 791198, Murchison, and Jbilet Winselwan, only very few barely visible fragments were observed from which the compositions of the TCIs were obtained. The sample from Jbilet Winselwan shows a large range of the "FeO"/SiO_2 versus S/SiO_2 ratios for the two TCI-rich fragments, which can be classified as subtypes of CM2.4 to CM2.9, while the TCIs of the host lithology are more homogeneous and have a composition consistent with a subtype classification of CM2.5. Within the nearly unbrecciated CM chondrite Y-791198, only one barely

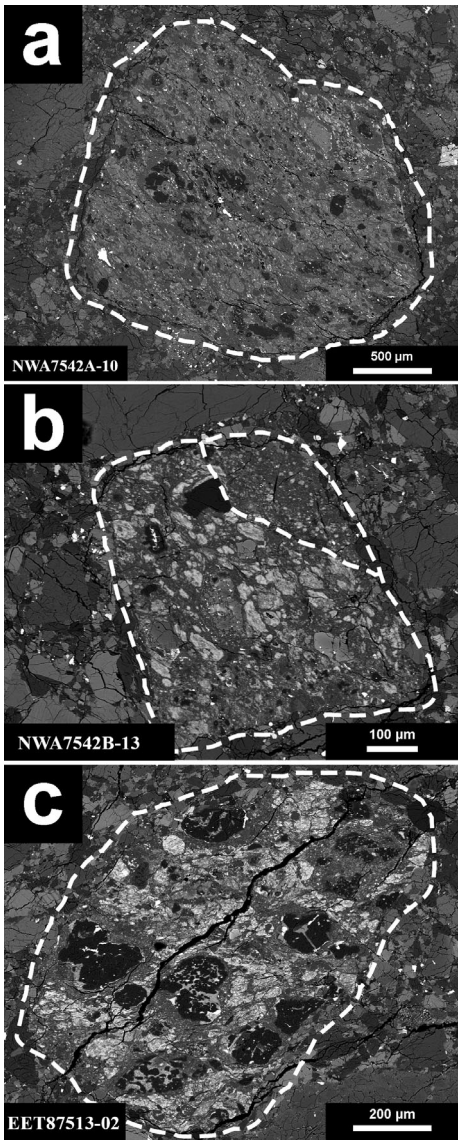

Fig. 9. CM-type fragments with different degrees of alteration identified and measured in HED breccias: (a) NWA 7542A-10 (CM2.2); (b) NWA 7542B-13 (CM2.6); the fragment contains two lithologies as indicated by a dashed line, and (c) EET 87513,13-02 (CM2.6).

visible area (probably a fragment) was discernible, and this area's TCIs are chemically similar to fragments of subtype CM2.8 (Fig. 10; Table 2). A similar relationship is found for Murchison. The three visible fragments show a very low degree of aqueous alteration (CM2.9), while the main host rock lithology is of CM2.7.

During the random measurements of TCIs in the main host rock lithologies of Murchison, Y-791198, and Jbilet Winselwan, we found that the TCIs in the analyzed areas are not completely homogeneous. However, the variations are not as large as those within samples having clearly definable fragments of different degrees of alteration. The variations probably indicate impact-related mixing of fine-grained TCI-fragments within the (clastic) matrix of these three CM-rocks. The effect of impact-related mixing and, thus, "homogenization" is described well in Fig. 7 of Metzler et al. (1992).

CM Chondrites and Thermal Metamorphism of Related Samples

To be able to carry out a correct subclassification of a CM chondrite and their individual fragments, the effects of thermal metamorphism have to be considered. Thermal annealing is changing the textural, mineralogical, and chemical parameters of the chondrites and their individual clasts. In our study, WIS 91600 is recognized not to be a typical CM chondrite (Fig. S1 in supporting information). Optically, the sample does not contain TCI-bearing fragments or TCIs in the clastic matrix. The rock seems to have been influenced by a secondary process like thermal metamorphism. Already Rubin et al. (2007) described WIS 91600 as a thermally metamorphosed CM-like chondrite. Details on several other heated carbonaceous chondrites have been reported (e.g., Tomeoka 1989; Tomeoka et al. 1989; Zolensky et al. 1989a, 1989b; Akai 1990a, 1990b, 1992; Bischoff and Metzler 1991; Ikeda 1992; Tonui et al. 2002, 2003, 2014; Nakamura 2005; Harries and Langenhorst 2013; Ebert et al. 2019). Recently, a large light CM-clast in the Murchison breccia was described (Kerraouch et al. 2018; Bischoff et al. 2018a; Fig. 11). A detailed study shows that this clast having a granoblastic texture formed by metasomatic processes in the depth of a CM parent body (Kerraouch et al. 2019a). In the past, also CV chondrites and their dark inclusions were discussed as objects that suffered aqueous alteration and dehydration in their evolution (e.g., Bischoff et al. 1988; Krot et al. 2004).

For more information and detailed descriptions of the effects of thermal metamorphism on CM chondrites, the work of Tonui et al. (2014) is suggested to the reader.

Results of this Work Compared to those of Rubin et al. (2007)

The classification of CM chondrites suggested by Rubin et al. (2007) and the classification in this study are different (Fig. 12). Rubin et al. (2007) classified CM2 subtypes based on the abundance and size of serpentine-tochilinite intergrowths/PCPs (TCIs), on the "FeO"/SiO_2 ratio of the TCIs, as well as on the abundances (and types) of Ca-carbonates and metals. Furthermore, they classify CM2 subtypes based on the dominating petrologic type of fragments, which results in the highest subtype CM2.6. In this study, CM2 chondrites are classified solely based on the "FeO"/SiO_2

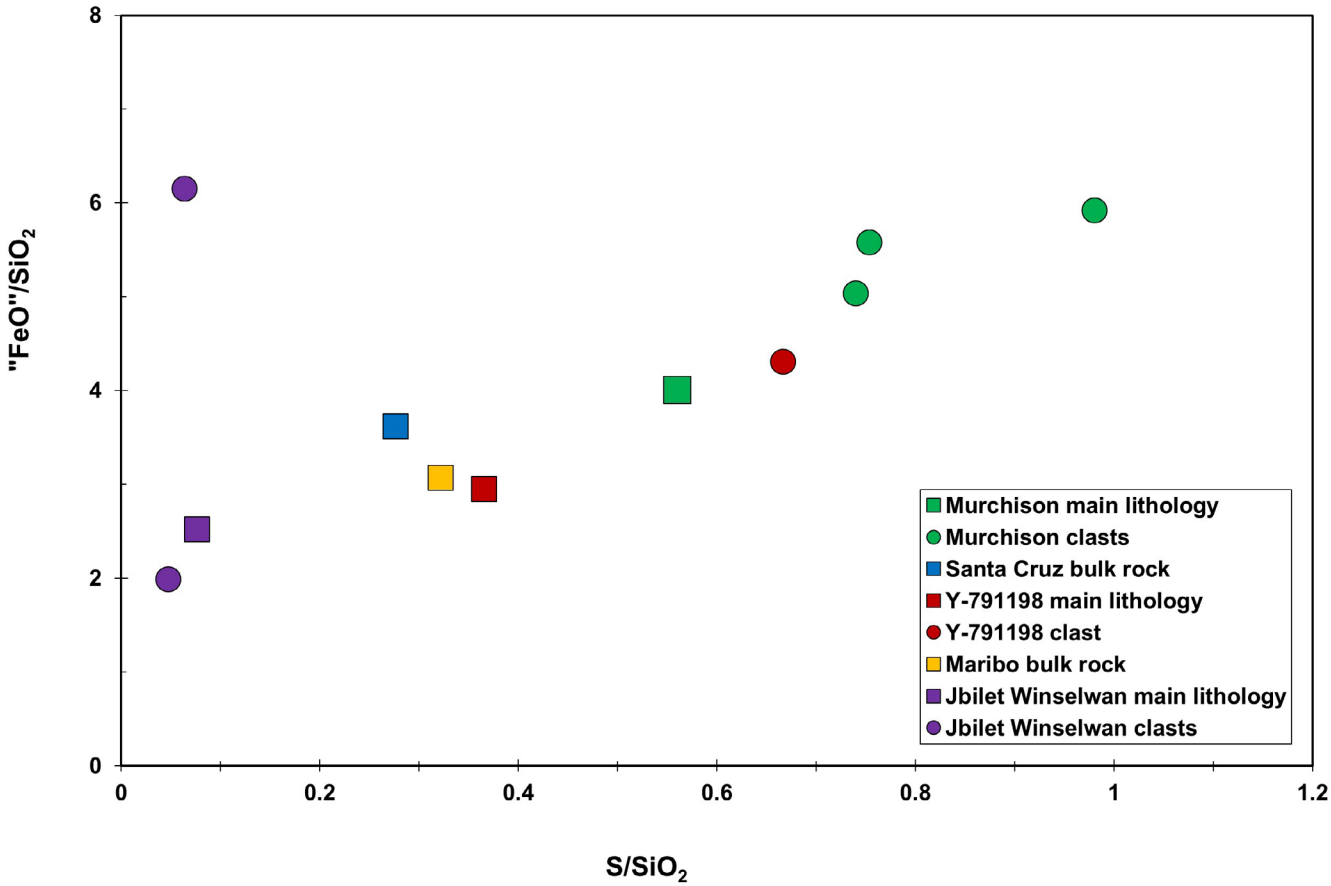

Fig. 10. "FeO"/SiO_2 versus S/SiO_2 for TCIs in samples with no or barely visible fragments. In the latter case, the TCI ratios of the main lithology (typically of the (clastic) matrix) are plotted. The TCI analyses of the clasts and the corresponding main lithology of a CM chondrite breccia are plotted in the same color.

ratio defined by Rubin et al. (2007), and we take into account the minimum and maximum degree of alteration of different fragments (Bischoff et al. 2017). As subtypes CM > 2.6 are not considered in the classification scheme of Rubin et al. (2007), this study proposes three further subtypes of CM2.7-CM2.9 for individual clasts in CM breccias. However, the Paris breccia has to be mentioned, for which Rubin (2015) determined a high "FeO"/SiO_2 ratio and suggested a subtype classification of at least CM2.7. As thin sections from Nogoya, Cold Bokkeveld, Murchison, and Y-791198 were part of the classification work of both studies (Rubin et al. [2007] and this study), we show a comparison of the results in Fig. 12.

Figure 12 illustrates clearly the difference between the classifications of Rubin et al. (2007) and those in this study. This is especially the case considering the CM breccias Murchison and Y-791198. The very different results indicate that Rubin et al. (2007) must have studied completely different lithologies than those studied in this work. This is not surprising: As known from meteorite breccias, the main fragment can vary from one thin section to another, and individual samples can even show different subtypes, as described by Bischoff et al. (2017). One good example is LON 94101 from which several thin sections were investigated. In most sections, fragments occur that show a large range of subtypes from CM2.0 to CM2.8 (Fig. 1). One sample (LON 94101-Cari 6) appears to be quite homogeneous, with some fragments of subtype CM2.2 (Table 2). Another good example is Nogoya (Fig. 3), which is classified as a CM2.2 by Rubin et al. (2007) based on the degree of alteration of the dominating lithology in their studied thin section. The thin section from this work also contains a fragment with the subclassification of CM2.2 (fragment B; Fig. 3), but the main fragment clearly is of petrologic type CM2.5 (fragment A; Fig. 3).

Based on the complex nature of CM breccias, this study proposes an extended subtype classification

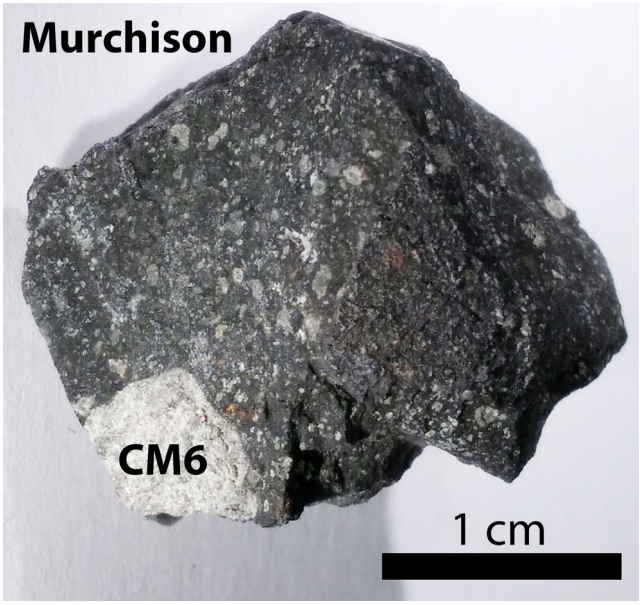

Fig. 11. The centimeter-sized light clast in the Murchison breccia has been identified as a strongly metamorphosed, type 6 lithology of a CM parent body. Figure modified after Bischoff et al. (2018a).

scheme (CM2.0-CM2.9; Table 3) and includes the characteristic of individual fragments into the classification in a similar way as done for ordinary chondrite breccias (Bischoff et al. 2017, 2018b) in order to appropriately account for the complexity of the CM chondrite breccias. Clear differences in the classification (e.g., Y-791198; Fig. 12) may be due to large-scale differences in the petrologic properties of the rock (as an effect of sampling during thin section preparation).

Genetic Relationship of CM-Like Clasts in HED Breccias and CM Chondrites

Several of the CM-like clasts in brecciated achondrites consist of different lithologies themselves, where they sample the border of two lithologies of different petrologic type. This resembles the brecciated nature of common CM2 chondrites as discussed in this work. They also span a range in petrologic subtypes from 2.2 to 2.8. Additionally, the genetic relation between CM-like clasts in HEDs and common CM chondrites is evidenced not only by their typical mineralogy but also by their D/H ratios, oxygen isotopes, and ε^{54}Cr composition (e.g., Buchanan et al. 1993; Gounelle et al. 2005; Van Drongelen et al. 2016; Patzek et al. 2018a, 2018b; 2019a, 2019b, 2020). Since many of the CM2-like clasts show no evidence for intensive heating or shattered structures, high-velocity impacts of larger impactors were not likely the major process of delivery to the HED parent bodies. Rather, the material was delivered via low-velocity impacts that mixed the clasts into the regolith of the HED parent body (e.g., Reddy et al. 2012). Features indicative for post-shock heating and shock are rare, which implies that low-impact velocities in combination with the general porous nature of carbonaceous chondrite material are the relevant process for delivery of CM material to the HED parent body. Furthermore, studies on the shock effects of carbonaceous chondrites have shown that most CM chondrites are unshocked or very weakly shocked (Scott et al. 1992), which is consistent with the observation of the CM-like clasts in HEDs. Nonetheless, heating features are observable in the fine-grained, phyllosilicate-rich matrix using TEM techniques (Buchanan et al. 1993). Also, Rubin and Bottke (2009) studied CM-like clasts in breccias and showed that clast PV3 from Plainview appears to have lost serpentine during its impact on the H-chondrite parent asteroid indicating a high impact velocity. Overall though, it is likely that most of the CM-like clasts in HEDs were incorporated into the host rock by slow infall of (micro)meteorites rather than by high-velocity impacts, since some are apparently not heated or fractured (Gounelle et al. 2003; Patzek et al. 2018a).

Brecciated CM Chondrites as Analogs for the Asteroidal Samples Returned by the OSIRIS-REx and Hayabusa 2 Missions

CI and CM chondrites (as also shown in this study) are highly brecciated rocks (e.g., Metzler et al. 1992; Bischoff et al. 2006, 2017; Morlok et al. 2006; Lindgren et al. 2013; Zolensky et al. 2015, 2017; Alfing et al. 2019). The characterization of CM breccias gives insight into the formation processes of CM parent bodies as well as into the evolution of asteroid surfaces. Considering the current NASA and JAXA missions to the asteroids (101955) Bennu and (162173) Ryugu, respectively, the microscopic observations on CI and CM chondrites may help to decipher distinct surface features on Bennu and Ryugu. Both asteroids are regarded as consisting of materials affected by aqueous alteration (e.g., Hamilton et al. 2019; Kitazato et al. 2019). Ryugu is described as a rubble pile-like body with a very low density and an estimated high porosity of >50% in its interior (Watanabe et al. 2019). Early spectral data of OSIRIS-REx show evidence for abundant hydrated minerals on the surface of Bennu as demonstrated by the near-infrared absorption at ~2.7 μm (Hamilton et al. 2019). These authors also state that the thermal infrared spectral features are most

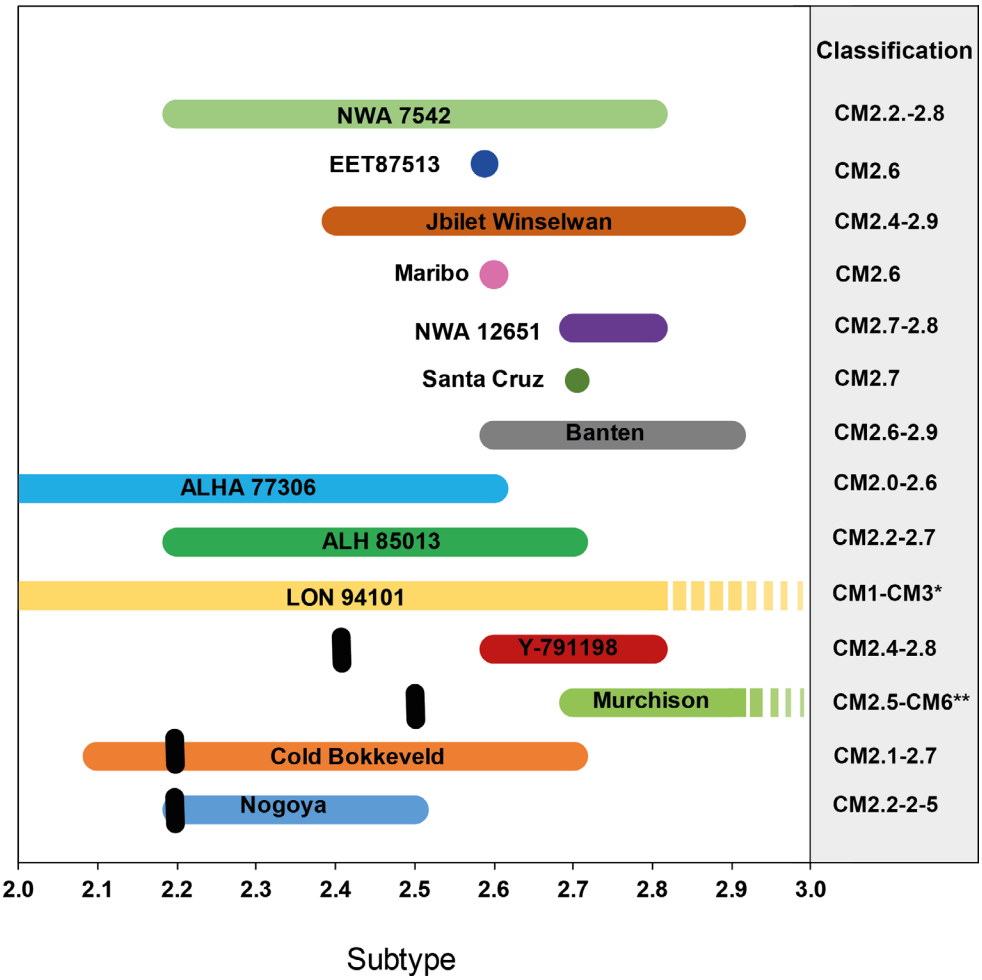

Fig. 12. CM classifications and comparison with results published by Rubin et al. (2007); the black bars represent the petrologic subtype as defined by Rubin et al. (2007) and the colored areas show the range defined in this work by taking into account differently altered lithologies. Since the thin sections studied here are different from those analyzed by Rubin et al. (2007), the different results may be due to large-scale differences in the petrologic properties of the bulk rocks. This must especially be the case considering the CM breccias Murchison and Y-791198. * As shown in Fig. 3, LON 94101 may also contain C1- and C3-related clasts; ** considering the CM6-clast (Bischoff et al. 2018a; Kerraouch et al. 2019a,2019b).

similar to those of aqueously altered CM-type carbonaceous chondrites. In addition, the low density of Bennu is consistent with a rubble-pile structure of high porosity assuming a particle density characteristic of CM chondrites (Lauretta et al. 2019). Fractured boulders as shown on surface images (Lauretta et al. 2019; McCoy et al. 2019)—clearly demonstrating surface rock heterogeneities—have morphologies that suggest the influence of impact or thermal processes. Considering Bennu as a possible CM parent body, the latter would not be surprising, since some CM chondrites available for study completely lost their volatiles due to heating or contain fragments that were formed in water-free environments or were strongly metamorphosed as shown by the centimeter-sized light clast in Murchison (Fig. 11) that has been identified as a type 6 lithology of a CM parent body (Kerraouch et al. 2018, 2019a, 2019b; Bischoff et al. 2018a). In summary, the mineralogical, textural, and chemical work on CM and CI breccias will certainly help to evaluate and understand the hopefully returned samples from the OSIRIS-REx and Hayabusa 2 missions.

CONCLUSION

In this study, a large number of TCI-rich fragments/areas from 27 thin sections out of 19 different CM chondrites and three brecciated HEDs were examined in order to reveal information on their brecciation processes and on the degree of aqueous

alteration of their individual clasts. According to the scheme of Rubin et al. (2007), 80 fragments, main lithologies, and bulk rocks were classified by determination of the "FeO"/SiO_2 ratios of the TCIs. New subtypes (CM2.7-CM2.9) were defined in this study to allow for a precise classification of samples with a low degree of aqueous alteration.

Most studied CM chondrite breccias contain individual fragments which are affected by various degrees of aqueous alteration (Fig. 12). The abundances of different clasts with different degrees of aqueous alteration can vary from thin section to thin section, even if the thin sections are from the same CM chondrite rock. Therefore, this study proposes an extended classification scheme based on that of Rubin et al. (2007) but includes the fragments with the highest and lowest degree of alteration in the classification (e.g., CM2.3-2.7, CM2.0-2.8, etc.). This type of classification includes the brecciation characteristics and is similar to the classification of ordinary chondrites (e.g., H3-5; L4-6, etc.). Good examples are the CM chondrites LON 94101 (CM2.0-2.8; clearly even more complex considering the fragments shown in Fig. 3), Cold Bokkeveld (CM2.1-2.7), and Nogoya (CM2.2-2.5).

Furthermore, fragments exist in which the TCIs show a higher degree of aqueous alteration based on the "FeO"/SiO_2 ratios than as indicated by their S/SiO_2 ratios. This might be due to a redistribution of sulfur during the aqueous alteration. Also, the low S/SiO_2 ratio of the TCIs could be related to the alteration of different precursor materials that were S-free phases (like metals). Thus, the "FeO"/SiO_2 ratio of TCIs is more reliable than S/SiO_2 as a parameter for subtype classification of CM chondrites and their fragments.

Acknowledgments—We thank Ulla Heitmann for sample preparation; Jasper Berndt-Gerdes and Beate Schmitte for analytical assistance; C. Brennecka for editorial support; as well as Alan Rubin, an anonymous reviewer, and the Associate Editor Tim Fagan for their helpful comments and suggestions. This work is funded by the Deutsche Forschungsgemeinschaft (DFG, German Research Foundation)—Project-ID 263649064—TRR 170 (subproject B05; AB). This is TRR170 publication no. 91. We also thank the Meteorite Working Group and Mike Zolensky (both Houston) as well as the NIPR (Tokio) for the loan of meteorite samples.

Editorial Handling—Dr. Timothy Fagan

REFERENCES

Akai J. 1990a. Mineralogical evidence of heating events in Antarctic carbonaceous chondrites, Y-86720 and Y-82162. *Proceedings of the NIPR Symposium on Antarctic Meteorites* 3:55–68.

Akai J. 1990b. Thermal metamorphism in four Antarctic carbonaceous chondrites and its temperature scale estimated by T-T-T diagram. *Proceedings of the NIPR Symposium on Antarctic Meteorites* 15:86–87.

Akai J. 1992. TTT-diagram of serpentine and saponite, and estimation of metamorphic heating degree of Antarctic carbonaceous chondrites. *Proceedings of the NIPR Symposium on Antarctic Meteorites* 5:120–135.

Alexander C. M. O'D., Bowden R., Fogel M. L., Howard K. T., Herd C. D. K., and Nittler L. R. 2012. The provenances of asteroids, and their contributions to the volatile inventories of the terrestrial planets. *Science* 337:721–723.

Alexander C. M. O'D., Howard K. T., Bowden R., and Fogel M. L. 2013. The classification of CM and CR chondrites using bulk H, C and N abundances and isotopic compositions. *Geochimica et Cosmochimica Acta* 123:244–260.

Alfing J., Patzek M., and Bischoff A. 2019. Modal abundances of coarse-grained (>5 μm) components within CI-chondrites and their individual clasts—Mixing of various lithologies on the CI parent body(ies). *Geochemistry—Chemie der Erde* 79:125532.

Bischoff A. 1998. Aqueous alteration of carbonaceous chondrites: Evidence for preaccretionary alteration—A review. *Meteoritics & Planetary Science* 33:1113–1122.

Bischoff A. and Metzler K. 1991. Mineralogy and petrography of the anomalous carbonaceous chondrites Yamato-86720, Yamato-82162, and Belgica-7904. *Proceedings of the NIPR Symposium on Antarctic Meteorites* 4:226–246.

Bischoff A., Palme H., Spettel B., Clayton R. N., and Mayeda T. K. 1988. The chemical composition of dark inclusions from the Allende meteorite. 19th Lunar and Planetary Science Conference. pp. 88–89.

Bischoff A., Scott E. R. D., Metzler K., and Goodrich C. A. 2006. Nature and origins of meteoritic breccias. In *Meteorites and the early solar system II*, edited by Lauretta D. S. and McSween H. Y. Jr. Tucson, Arizona: The University of Arizona Press. pp. 679–712.

Bischoff A., Ebert S., Metzler K., and Lentfort S. 2017. Breccia classification of CM chondrites (abstract #6089). *Meteoritics & Planetary Science* 52:A26.

Bischoff A., Patzek M., Ebert S., Pack A., Kerraouch I., and Zolensky M. E. 2018a. A large, light fragment in the Murchison (CM) breccia—A unique, highly-metamorphosed chondrite as a xenolith in a CM chondrite (abstract #6217). *Meteoritics & Planetary Science* 53:6217.

Bischoff A., Schleiting M., Wieler R., and Patzek M. 2018b. Brecciation among 2280 ordinary chondrites—Constraints on the evolution of their parent bodies. *Geochimica et Cosmochimica Acta* 238:516–541.

Brearley A. J. 2006. The action of water. In *Meteorites and the early solar system II*, edited by Lauretta D. S. and McSween H. Y. Jr. Tucson, Arizona: The University of Arizona Press. pp. 587–624.

Browning L. B., McSween H. Y. Jr., and Zolensky M. E. 1996. Correlated alteration effects in CM carbonaceous chondrites. *Geochimica et Cosmochimica Acta* 60:2621–2633.

Buchanan P. C., Zolensky M. E., and Reid A. M. 1993. Carbonaceous chondrite clasts in the howardites Bholghati and EET87513. *Meteoritics & Planetary Science* 28:659–669.

Ebert S., Bischoff A., Harries D., Lentfort S., Barrat J.-A., Pack A., Gattacceca J., Visser R., Schmid-Beurmann P., and Kimpel S. 2019. Northwest Africa 11024—A heated and dehydrated unique carbonaceous (CM) chondrite. *Meteoritics & Planetary Science* 54:328–356.

Ebert S., Patzek M., Lentfort S., and Bischoff A. 2020. Accretion of differentiated achondritic and aqueously-altered chondritic materials in the early solar system—Significance of an igneous fragment in the CM chondrite NWA 12651. *Meteoritics & Planetary Science* 54:2985–2995.

Endress M. and Bischoff A. 1993. Mineralogy, degree of brecciation, and aqueous alteration of CI chondrites Orgueil, Ivuna, and Alais (abstract). *Meteoritics* 28:345–346.

Fodor R. V. and Keil K. 1976. Carbonaceous and non-carbonaceous lithic fragments in Plainview, Texas, chondrite: Origin and history. *Geochimica et Cosmochimica Acta* 40:177–189.

Fredriksson K. and Kerridge J. F. 1988. Carbonates and sulfates in CI chondrites: Formation by aqueous activity on the parent body. *Meteoritics* 23:35–44.

Fuchs L. H., Olsen E., and Jensen K. J. 1973. Mineralogy, mineral-chemistry, and composition of the Murchison (C2) meteorite. *Smithsonian Contributions to the Earth Science* 10:1–39.

Garenne A., Beck P., Montes-Hernandez G., Chiriac R., Toche F., Quirico E., Bonal L., and Schmitt B. 2014. The abundance and stability of "water" in type 1 and 2 carbonaceous chondrites (CI, CM and CR). *Geochimica et Cosmochimica Acta* 137:93–112.

Gounelle M., Zolensky M. E., Liou J.-C., Bland P. A., and Alard O. 2003. Mineralogy of carbonaceous chondritic microclasts in howardites: Identification of C2 fossil micrometeorites. *Geochimica et Cosmochimica Acta* 67:507–527.

Gounelle M., Engrand C., Alard O., Bland P. A., Zolensky M. E., Russell S. S., and Duprat J. 2005. Hydrogen isotopic composition of water from fossil micrometeorites in howardites. *Geochimica et Cosmochimica Acta* 69:3431–3443.

Grimm R. E. and Mcsween H. Y. Jr 1989. Water and the thermal evolution of carbonaceous chondrite parent bodies. *Icarus* 82:244–280.

Hamilton V. E., Simon A. A., Christensen P. R., Reuter D. C., Clark B. E., Barucci M. A., Bowles N. E., Boynton W. V., Brucato J. R., Cloutis E. A., Connolly H. C., Donaldson Hanna K. L., Emery J. P., Enos H. L., Fornasier S., Haberle C. W., Hanna R. D., Howell E. S., Kaplan H. H., Keller L. P., Lantz C., Li J.-Y., Lim L. F., McCoy T. J., Merlin F., Nolan M. C., Praet A., Rozitis B., Sandford S. A., Schrader D. L., Thomas C. A., Zou X.-D., Lauretta D. S., and Osiris-Rex Team. 2019. Evidence for widespread hydrated minerals on asteroid (101955) Bennu. *Nature Astronomy* 3:332–340.

Harries D. and Langenhorst F. 2013. The nanoscale mineralogy of Fe, Ni sulfides in pristine and metamorphosed CM and CM/CI-like chondrites: Tapping a petrogenetic record. *Meteoritics & Planetary Science* 48:879–903.

Howard K. T., Benedix G. K., Bland P. A., and Cressey G. 2009. Modal mineralogy of CM2 chondrites by X-ray diffraction (PSD-XRD). Part 1: Total phyllosilicate abundance and the degree of aqueous alteration. *Geochimica et Cosmochimica Acta* 73:4576–4589.

Ikeda Y. 1992. An overview of the research consortium, "Antarctic carbonaceous chondrites with CI affinities, Yamato-86720, Yamato-82162, and Belgica-7904." *Proceedings of the NIPR Symposium on Antarctic Meteorites* 5:49–73.

Johnson C. A., and Prinz M. 1993. Carbonate compositions in CM and CI chondrites and implications for aqueous alteration. *Geochimica et Cosmochimica Acta* 57:2843–2852.

Kerraouch I., Zolensky M. E., Bischoff A., Le L., Belhaï D., Patzek M., and Ebert S. 2018. Mineralogical study of a white clast from Murchison (CM2): Comparison with R chondrites (abstract #6363). *Meteoritics & Planetary Science* 53:6363.

Kerraouch I., Ebert S., Patzek M., Bischoff A., Zolensky M. E., Pack A., Schmitt-Kopplin P., Belhai D., Bendaoud A., and Le L. 2019a. A light, chondritic xenolith in the Murchison (CM) chondrite—Formation by fluid-assisted percolation during metasomatism? *Geochemistry—Chemie der Erde* 79:125518.

Kerraouch I., Bischoff A., Zolensky M. E., Ebert S., Patzek M., Pack A., Schmitt-Kopplin P., Belhai D., Bendaoud A., and Le L. 2019b. A chondritic xenolith in the Murchison (CM2) chondrite formed by fluid-assisted percolation during metasomatism (abstract #6197). 54th Lunar and Planetary Science Conference. CD-ROM.

Kitazato K., Milliken R. E., Iwata T., Abe M., Ohtake M., Matsuura S., Arai T., Nakauchi Y., Nakamura T., Matsuoka M., Senshu H., Hirata N., Hiroi T., Pilorget C., Brunetto R., Poulet F., Riu L., Bibring J.-P., Takir D., Domingue D. L., Vilas F., Barucci M. A., Perna D., Palomba E., Galiano A., Tsumura K., Osawa T., Komatsu M., Nakato A., Arai T., Takato N., Matsunaga T., Takagi Y., Matsumoto K., Kouyama T., Yokota Y., Tatsumi E., Sakatani N., Yamamoto Y., Okada T., Sugita S., Honda R., Morota T., Kameda S., Sawada H., Honda C., Yamada M., Suzuki H., Yoshioka K., Hayakawa M., Ogawa K., Cho Y., Shirai K., Shimaki Y., Hirata N., Yamaguchi A., Ogawa N., Terui F., Yamaguchi T., Takei Y., Saiki T., Nakazawa S., Tanaka S., Yoshikawa M., Watanabe S., and Tsuda Y. 2019. The surface composition of asteroid 162173 Ryugu from Hayabusa2 near-infrared spectroscopy. *Science* 364:272–275.

Krot A. N., Petaev M. I., and Bland P. A. 2004. Multiple formation mechanisms olivine in CV carbonaceous chondrites during fluid-assisted metamorphism. *Antarctic Meteorite Research* 17:153–171.

Lauretta D. S., Dellagiustina D. N., Bennett C. A., Golish D. R., Becker K. J., Balram-Knutson S. S., Barnouin O. S., Becker T. L., Bottke W. F., Boynton W. V., Campins H., Clark B. E., Connolly H. C., Drouet D'Aubigny C. Y., Dworkin J. P., Emery J. P., Enos H. L., Hamilton V. E., Hergenrother C. W., Howell E. S., Izawa M. R. M., Kaplan H. H., Nolan M. C., Rizk B., Roper H. L., Scheeres D. J., Smith P. H., Walsh K. J., Wolner C. W. V., and Team Osiris-Rex. 2019. The unexpected surface of asteroid (101955) Bennu. *Nature* 568:55–60.

Lentfort S., Bischoff A., and Ebert S. 2019. Classification of 13 CM chondrite breccias and CM clasts in two achondrites (abstract #6029). 54th Lunar and Planetary Science Conference. CD-ROM.

Lindgren P., Lee M. R., Sofe M. R., and Zolensky M. E. 2013. Clasts in the CM2 carbonaceous chondrite Lonewolf Nunataks 94101: Evidence for aqueous alteration prior to complex mixing. *Meteoritics & Planetary Science* 48:1074–1090.

Mackinnon I. D., and Zolensky M. E. 1984. Proposed structures for poorly characterized phases in C2M carbonaceous chondrite meteorites. *Nature* 309:240–242.

McCoy T. J., Connolly H. C. Jr., Corrigan C. M., Jawin E. R., Sandford S., Molaro J., DellaGiustina D. N., Rizk B., Nolan M. C., and Lauretta D. S. and the OSIRIS-REx Team. 2019. Brecciated boulders: Evidence for impact mixing on Bennu's parent body (abstract #6428). 54th Lunar and Planetary Science Conference. CD-ROM.

McSween H. Y. Jr. 1979a. Are carbonaceous chondrites primitive or processed? A review. *Reviews of Geophysics* 17:1059–1078.

McSween H. Y. Jr. 1979b. Alteration in CM carbonaceous chondrites inferred from modal and chemical variations in matrix. *Geochimica et Cosmochimica Acta* 43:1761–1770.

Meteoritical Bulletin Database. https://www.lpi.usra.edu/meteor/metbull.php. Accessed December 10, 2019.

Metzler K. and Bischoff A. 1996. Constraints on chondrite agglomeration from fine-grained chondrule rims. In *Chondrules and the protoplanetary disk*, edited by Hewins R. H., Jones R. H., and Scott E. R. D. Cambridge, UK: Cambridge University Press. pp. 153–162.

Metzler K., Bischoff A., and Stöffler D. 1992. Accretionary dust mantles in CM-chondrites: Evidence for nebula processes. *Geochimica et Cosmochimica Acta* 56:2873–2897.

Metzler K., Bischoff A., Greenwood R. C., Palme H., Gellissen M., Hopp J., Franchi I. A., and Trieloff M. 2011. The L3–6 chondritic regolith breccia Northwest Africa (NWA) 869: (I) Petrology, chemistry, oxygen isotopes, and Ar-Ar age determinations. *Meteoritics & Planetary Science* 46:652–680.

Morlok A., Bischoff A., Stephan T., Floss C., Zinner E. K., and Jessberger E. K. 2006. Brecciation and chemical heterogeneities of CI chondrites. *Geochimica et Cosmochimica Acta* 70:5371–5394.

Müller W. F., Kurat G., and Kracher A. 1979. Chemical and crystallographic study of cronstedtite in the matrix of the Cochabamba (CM2) carbonaceous chondrite. *Tschermaks Mineralogische und Petrographische Mitteilungen* 26:293–304.

Nakamura T. 2005. Post-hydration thermal metamorphism of carbonaceous chondrites. *Journal of Mineralogical and Petrological Science* 100:260–272.

Patzek M., Bischoff A., Visser R., and John T. 2018a. Mineralogy of volatile-rich clasts in brecciated meteorites. *Meteoritics & Planetary Science* 53:2519–2540.

Patzek M., Pack A., Bischoff A., Visser R., and John T. 2018b. O-isotope composition of CI- and CM-like clasts in ureilites, HEDs, and CR chondrites (abstract 6254). *Meteoritics & Planetary Science* 53:6254.

Patzek M., Bischoff A., Hoppe P., Pack A., Visser R., and John T. 2019a. Oxygen and hydrogen isotopic evidence for the existence of several C1 parent bodies in the early solar system (abstract# 1779). 50th Lunar and Planetary Science Conference. CD-ROM.

Patzek M., Kadlag Y., Bischoff A., Visser R., Becker H., and John T. 2019b. Chromium isotopes and trace element concentration of xenolithic C1 clasts in brecciated chondrites and achondrites (abstract #6027). 54th Lunar and Planetary Science Conference. CD-ROM.

Patzek M., Hoppe P., Bischoff A., Visser R., and John T. 2020. Hydrogen isotopic composition of CI- and CM-like clasts from meteorite breccias—Sampling unknown sources of carbonaceous chondrite material. *Geochimica et Cosmochimica Acta* 272:177–197.

Ramdohr P. 1963. The opaque minerals in stony meteorites. *Journal of Geophysical Research* 68:2011–2036.

Reddy V., Le Corre L., O'Brien D. P., Nathues A., Cloutis E. A., Durda D. D., Bottke W. F., Bhatt M. U., Nesvorny D., and Buczkowski D. 2012. Delivery of dark material to Vesta via carbonaceous chondritic impacts. *Icarus* 221:544–559.

Rubin A. E. 2015. An American on Paris: Extent of aqueous alteration of a CM chondrite and the petrography of its refractory and amoeboid olivine inclusions. *Meteoritics & Planetary Science* 50:1595–1612.

Rubin A. E. and Bottke W. F. 2009. On the origin of shocked and unshocked CM clasts in H-chondrite regolith breccias. *Meteoritics & Planetary Science* 44:701–724.

Rubin A. E. and Wasson J. T. 1986. Chondrules in the Murray CM2 meteorite and compositional differences between CM-CO and ordinary chondrite chondrules. *Geochimica et Cosmochimica Acta* 50:307–315.

Rubin A. E., Trigo-Rodríguez J. M., Huber H., and Wasson J. T. 2007. Progressive aqueous alteration of CM carbonaceous chondrites. *Geochimica et Cosmochimica Acta* 71:2361–2382.

Scott E. R., Keil K., and Stoeffler D. 1992. Shock metamorphism of carbonaceous chondrites. *Geochimica et Cosmochimica Acta* 56:4281–4293.

Tomeoka K. 1989. Belgica-7904: A new kind of carbonaceous chondrite from Antarctica: Mineralogy and petrology. *Proceedings of the NIPR Symposium on Antarctic Meteorites* 14:18–20.

Tomeoka K. and Buseck P. 1988. Matrix mineralogy of the Orgueil CI carbonaceous chondrite. *Geochimica et Cosmochimica Acta* 52:1627–1640.

Tomeoka K., Kojima H., and Yanai K. 1989. Yamato-86720: A CM carbonaceous chondrite having experienced extensive aqueous alteration and thermal metamorphism. *Proceedings of the NIPR Symposium on Antarctic Meteorites* 2:55–74.

Tonui E. K., Zolensky M. E., and Lipschutz M. E. 2002. Petrography, mineralogy and trace element chemistry of Yamato-86029, Yamato-793321 and Lewis Cliff 85332: Aqueous alteration and heating events. *Antarctic Meteorite Research* 15:38–58.

Tonui E. K., Zolensky M. E., Lipschutz M. E., Wang M., and Nakamura T. 2003. Yamato 86029: Aqueously altered and thermally metamorphosed CI chondrite with unusual textures. *Meteoritics & Planetary Science* 38:269–292.

Tonui E., Zolensky M., Hiroi T., Nakamura T., Lipschutz M., Wang M.-S., and Okudaira K. 2014. Petrographic, chemical and spectroscopic evidence for thermal metamorphism in carbonaceous chondrites I: CI and CM chondrites. *Geochimica et Cosmochimica Acta* 126:284–306.

Van Drongelen K. D., Rumble D. III, and Tait K. T. 2016. Petrology and oxygen isotopic compositions of clasts in HED polymict breccia NWA 5232. *Meteoritics & Planetary Science* 51:1184–1200.

Visser R., John T., Menneken M., Patzek M., and Bischoff A. 2018. Temperature constraints by Raman spectroscopy of organic matter in volatile-rich clasts and

carbonaceous chondrites. *Geochimica et Cosmochimica Acta* 241:38–55.

Watanabe S., Hirabayashi M., Hirata N., Na Hirata R., Noguchi Y. Shimaki, Ikeda H., Tatsumi E., Yoshikawa M., Kikuchi S., Yabuta H., Nakamura T., Tachibana S., Ishihara Y., Morota T., Kitazato K., Sakatani N., Matsumoto K., Wada K., Senshu H., Honda C., Michikami T., Takeuchi H., Kouyama T., Honda R., Kameda S., Fuse T., Miyamoto H., Komatsu G., Sugita S., Okada T., Namiki N., Arakawa M., Ishiguro M., Abe M., Gaskell R., Palmer E., Barnouin O. S., Michel P., French A. S., McMahon J. W., Scheeres D. J., Abell P. A., Yamamoto Y., Tanaka S., Shirai K., Matsuoka M., Yamada M., Yokota Y., Suzuki H., Yoshioka K., Cho Y., Nishikawa N., Sugiyama T., Kikuchi H., Hemmi R., Yamaguchi Tomohiro, Naoko Ogawa G., Ono Yuya Mimasu, Yoshikawa K., Takahashi T., Takei Y., Atsushi F. C., Hirose T. I., Hayakawa M., Hosoda S., Mori O., Sawada H., Shimada T., Soldini S., Yano H., Tsukizaki R., Ozaki M., Yuichi I. K., Ogawa M. F., Ho T.-M., Moussi A., Jaumann R., Bibring J.-P., Krause C., Terui F., Saiki T., Nakazawa S., and Tsuda Y. 2019. Hayabusa2 arrives at the carbonaceous asteroid 162173 Ryugu—A spinning top–shaped rubble pile. *Science* 364:268–272.

Zolensky M. E., and McSween H. Y. Jr. 1988. Aqueous alteration. In *Meteorites and the early solar system*, edited by Kerridge J. F. and Matthews M. S. Tucson, Arizona: University of Arizona Press. pp. 114–143.

Zolensky M. E., Bourcier W. L., and Gooding J. L. 1989a. Aqueous alteration on the hydrated asteroids: Results of EQ3/6 computer simulations. *Icarus* 78:411–425.

Zolensky M. E., Barrett R. A., and Prinz M. 1989b. Petrography, mineralogy and matrix compositions of Yamato-82162, a new CI2 chondrite. *Proceedings Lunar and Planetary Science Conference* 20:1253–1254.

Zolensky M. E., Weisberg M. K., Buchanan P. C., and Mittlefehldt D. W. 1996. Mineralogy of carbonaceous chondrite clasts in HED achondrites and the Moon. *Meteoritics & Planetary Science* 31:518–537.

Zolensky M. E., Mittlefehldt D. W., Lipschutz M. E., Wang M., Clayton R. N., Mayeda T. K., Grady M. M., Pillinger C., and David B. 1997. CM chondrites exhibit the complete petrologic range from type 2 to 1. *Geochimica et Cosmochimica Acta* 61:5099–5115.

Zolensky M. E., Nakamura K., Gounelle M., Mikouchi T., Kasama T., Tachikawa O., and Tonui E. 2002. Mineralogy of Tagish Lake: An ungrouped type 2 carbonaceous chondrite. *Meteoritics & Planetary Science* 37:737–761.

Zolensky M. E., Gregory T., Takenouchi A., Nishiizumi K., Trieman A., Berger E., Le L., Fagan A., Velbel M., Imae N., Yamaguchi A., and Caffee M. 2015. CM carbonaceous chondrite lithologies and their space exposure ages (abstract). NIPR Symposium on Antarctic Meteorites 2015.

Zolensky M., Takenouchi A., Gregory T., Nishiizumi K., Caffee M., Velbel M., Ross K., Zolensky A., Le L., and Imae N. 2017. The relationship between cosmic-ray exposure ages and mixing of CM chondrite lithologies (abstract #2094). 48th Lunar and Planetary Science Conference. CD-ROM.

SUPPORTING INFORMATION

Additional supporting information may be found in the online version of this article.

Supplement S1. Anomalous Samples and Unique Fragments.

Fig. S1. BSE image of WIS 91600 having small magnetite inclusions and magnetite nests in the clastic matrix *Dhofar 225*. This anomalous CM rock seems to be modified by secondary processes (Fig. S2). In the beginning of this study, the sample was measured but later excluded from the classification because the measurements indicate that the samples did not contain real TCIs, but areas looking like TCIs turned out to be composed of sulfidic or metallic components rather than phyllosilicates. Another reason for excluding this meteorite is its oxygen isotope composition, which is more enriched in ^{17}O and ^{18}O than those of other CM chondrites and plots next to the Belgica group (see Meteoritical Bulletin Database; https://www.lpi.usra.edu/meteor/).

Fig. S2. Anomalous CM chondrite Dhofar 225: Bright areas that look like TCIs probably represent areas with abundant sulfidic or metallic components rather than phyllosilicates.

Fig. S3. BSE images of TCI-rich areas in (a) NWA 10907 and (b) NWA 10908: The light TCI-rich areas show very different optical characteristics compared with those shown in the CMs and their fragments in the main document (compare Figs. 4 and 5).

Fig. S4. BSE images of some fragments from Jbilet Winselwan, NWA 7542, and Sariçiçek having bright areas looking like TCIs, but contain sulfidic and/or metallic components.